# Unparalleled Ease of Access to a Library of Biheteroaryl Fluorophores via Oxidative Cross-Coupling Reactions: Discovery of Photostable NIR Probe for Mitochondria

Yangyang Cheng,[†] Gaocan Li,[‡] Yang Liu,[†] Yang Shi,[†] Ge Gao,*[,†] Di Wu,[†] Jingbo Lan,[†] and Jingsong You*[,†]

[†]Key Laboratory of Green Chemistry and Technology of Ministry of Education, College of Chemistry, and State Key Laboratory of Biotherapy, West China Hospital, West China Medical School, Sichuan University, 29 Wangjiang Road, Chengdu 610064, China
[‡]National Engineering Research Center for Biomaterials, Sichuan University, 29 Wangjiang Road, Chengdu 610064, China

Ⓢ *Supporting Information*
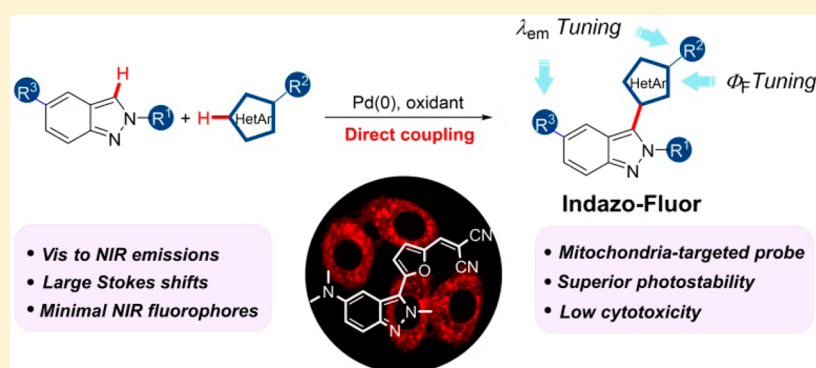
ABSTRACT: The development of straightforward accesses to organic functional materials through C−H activation is a revolutionary trend in organic synthesis. In this article, we propose a concise strategy to construct a large library of donor−acceptor-type biheteroaryl fluorophores via the palladium-catalyzed oxidative C−H/C−H cross-coupling of electron-deficient 2H-indazoles with electron-rich heteroarenes. The directly coupled biheteroaryl fluorophores, named Indazo-Fluors, exhibit continuously tunable full-color emissions with quantum yields up to 93% and large Stokes shifts up to 8705 cm^{-1} in CH$_2$Cl$_2$. By further fine-tuning of the substituent on the core skeleton, Indazo-Fluor 3l (FW = 274; λ_{em} = 725 nm) is obtained as the lowest molecular weight near-infrared (NIR) fluorophore with emission wavelength over 720 nm in the solid state. The NIR dye **5h** specifically lights up mitochondria in living cells with bright red luminescence. Typically, commercially available mitochondria trackers suffer from poor photostability. Indazo-Fluor **5h** exhibits superior photostability and very low cytotoxicity, which would be a prominent reagent for *in vivo* mitochondria imaging.

INTRODUCTION

Organic fluorophores are of great interest in diverse scientific fields like materials science, chemistry, and biology due to their high sensitivity, structural versatility, good specificity, high chemical stability, and synthetic accessibility.[1] Particularly, low-molecular-weight organic fluorophores are highly desirable for biological studies because of their unique advantages such as good cell permeability and minimal perturbation to living systems.[2] In recent years, near-infrared (NIR) fluorophores (emission wavelengths between 650 and 900 nm) have held the spotlight for *in vivo* bioanalysis and bioimaging owing to their minimal photodamage, low light scattering, and deep tissue penetration.[3] The development of novel minimal NIR fluorophores with structural petiteness is an appealing, yet significantly challenging task. Although a great number of small organic fluorophores have been reported, NIR fluorophores with molecular weight below 300 still remain scarce.[4]

Oxyluciferin is a typical bisazole molecule generated during the bioluminescence process found in firefly, accompanied by intense luminescence emission in a wide wavelength range of 530−640 nm when returning from the excited state to the ground state (Figure 1).[5] Recently, biheteroarenes have gradually become appealing building blocks to construct
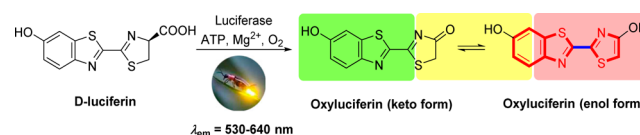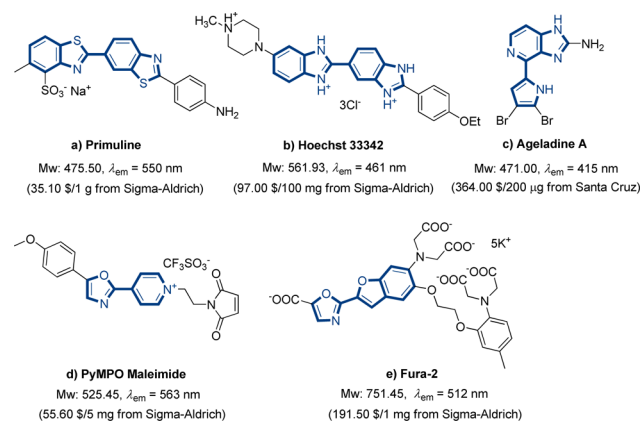

Figure 1. Oxyluciferin generated during the bioluminescence process in firefly.

fluorophores,[6] and a large number of fluorophores featuring biheteroaryl frameworks with peripherial functionalities are now commercially available (Scheme 1).[7] Considering that

Scheme 1. Selected Examples of Commercially Available Fluorescent Probes Containing Biheteroaryl Frameworks

a) Primuline
Mw: 475.50, λ_{em} = 550 nm
(35.10 $/1 g from Sigma-Aldrich)

b) Hoechst 33342
Mw: 561.93, λ_{em} = 461 nm
(97.00 $/100 mg from Sigma-Aldrich)

c) Ageladine A
Mw: 471.00, λ_{em} = 415 nm
(364.00 $/200 µg from Santa Cruz)

d) PyMPO Maleimide
Mw: 525.45, λ_{em} = 563 nm
(55.60 $/5 mg from Sigma-Aldrich)

e) Fura-2
Mw: 751.45, λ_{em} = 512 nm
(191.50 $/1 mg from Sigma-Aldrich)

tuning intramolecular charge transfer (ICT) through donor–acceptor (D–A) type molecular systems is a facile and efficient gateway in the discovery of full-color-tunable organic fluorophores,[8] the coupling between two heteroarenes with distinct electronic properties, i.e., electron-rich and electron-deficient, could enable a D–A type Het^{ER}–Het^{ED} skeleton (Figure 2). Attaching functional peripherals on biheteroarenes could allow further tuning of the ICT character to endow a wide region of fluorescence emissions.
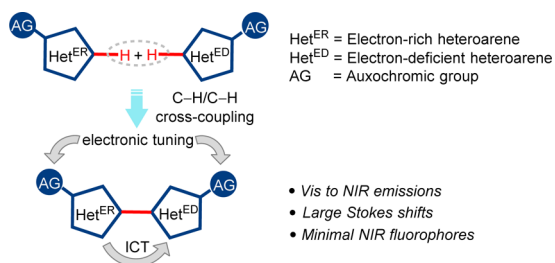

Het^{ER} = Electron-rich heteroarene
Het^{ED} = Electron-deficient heteroarene
AG = Auxochromic group

• Vis to NIR emissions
• Large Stokes shifts
• Minimal NIR fluorophores

Figure 2. Design and construction of biheteroaryl fluorescent skeletons via direct oxidative C–H/C–H cross-coupling reactions.

To understand the fluorescence–structure relationship,[9] it is particularly necessary to develop a simple and straightforward manner to assemble a large library of fluorophores with a broad range of emission wavelengths. Traditional cyclization and transition-metal-catalyzed C–X/C–M coupling reactions are common strategies to access biheteroaryl fluorophores.[6b,c,10] However, these protocols often suffer from tedious multistep synthesis including preactivation of substrates as well as general reluctance to the coupling partners with reactive functional groups, which limit rapid diversification toward fluorophores. Given that the emerging transition metal-catalyzed direct oxidative C–H/C–H cross-coupling reactions between two heteroarenes have shown the advantages of both the avoidance of tedious preactivation of starting materials and the tolerance of reactive functional groups,[11] it would be the most straightforward and convenient access to assemble a library of biheteroaryl fluorophores starting from easily available heteroarene substrates (Figure 2).[12]

As electron-deficient benzopyrazole molecules, indazoles that are privileged structural units with biological and pharmacological activities[13] have emerged as novel fluorescent skeletons in recent years.[14] In this work, we wish to demonstrate the power of oxidative C–H/C–H cross-coupling reaction in the rapid assembly of a small-molecule organic fluorophore library by taking the direct couple of 2H-indazoles with various electron-rich heteroarenes as an example. Through high-throughput screening of fluorophores, we aspire for the discovery of minimal NIR probes with superior photostability and low cytotoxicity.

■ RESULTS AND DISCUSSION

Molecular Design. Recently, Ellman and co-workers investigated the potential of 2-aryl-2H-indazole core skeleton as fluorophores by a rhodium(III)-catalyzed cyclization reaction between azobenzenes and aldehydes.[14c] The results show that electron variation at the N2 position (R^1) has very limited influence on the emissions, which are mainly located in the blue-light region of a narrow range from 398 to 438 nm. Considering that indazole is a common electron-deficient heteroarene, the coupling of indazole with typical electron-rich heteroarenes such as thiophene, furan, pyrrole, and indole could directly assemble Het^{ER}–Het^{ED} skeletons with ICT character. The density functional theory (DFT) calculation was then conducted to predict the position that can efficiently disturb the electronic effect on indazole. The results demonstrate that the C3 position of indazole has the largest electron density difference between LUMO and HOMO among the modifiable positions, suggesting that it would be a preferential site for the connection of Het^{ER}–Het^{ED} biheteroaryl skeletons (Figure 3a).[9b,d,15] In addition to the alterability
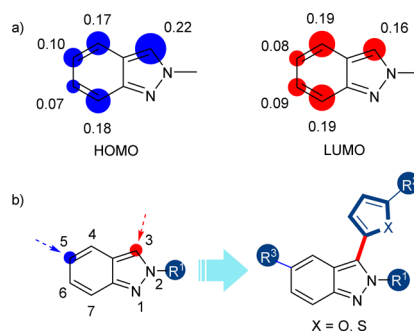

Figure 3. (a) HOMO and LUMO electron densities. The blue and red circle sizes represent the atomic contribution (only the modifiable carbon atoms are shown). (b) Selected positions of indazole motif to construct the biheteroaryl fluorophores.

of the electron-rich heteroaryl moiety, the R^3 group at the C5 position of indazole and the R^2 group on the electron-rich heteroaryl are also chosen for the study of fluorescence–structure relationship (Figure 3b). The variation of R^2 and R^3 groups would further tune the ICT character and provide a library of biheteroaryl fluorophores with divergent emissions.

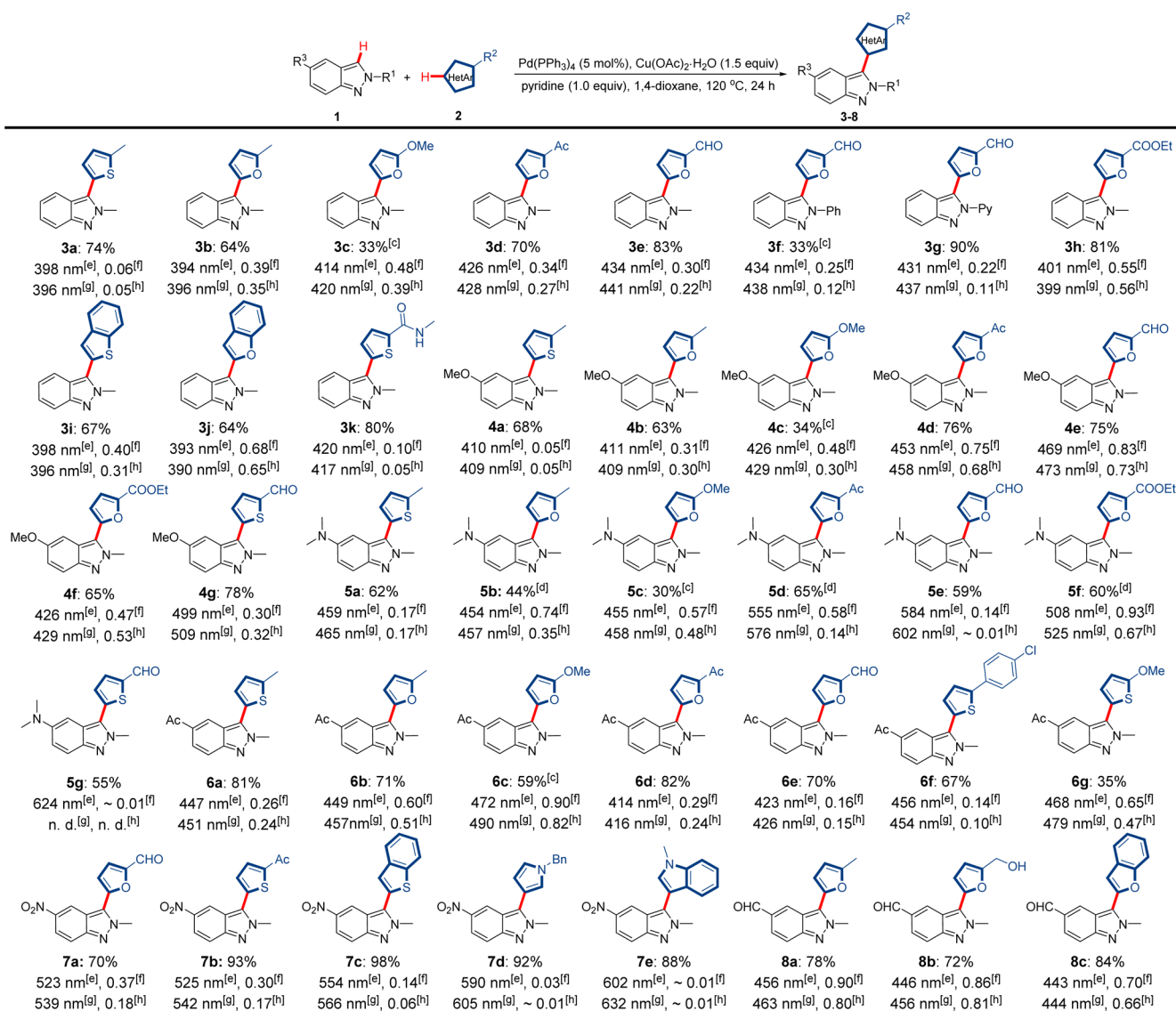**Methodology.** With this molecule design in mind, we aimed to develop a concise and rapid construction of a 3-heteroarylated 2H-indazole library. Recently, the direct C3–H heteroarylation of 2H-indazoles with electron-deficient heteroaryl halides such as halopyridine was performed to construct 3-heteroarylated 2H-indazoles (C–H/C–X type).[16] We herein initiated our investigation with the C–H/C–X cross-coupling

of 2-methyl-2H-indazole **1a** with 2-bromo-5-methylthiophene **2a′**. Unfortunately, the coupling reaction only gave a very low yield of the desired product **3a** (up to 11%) under several generally used catalytic conditions (eq 1 and Table S1).
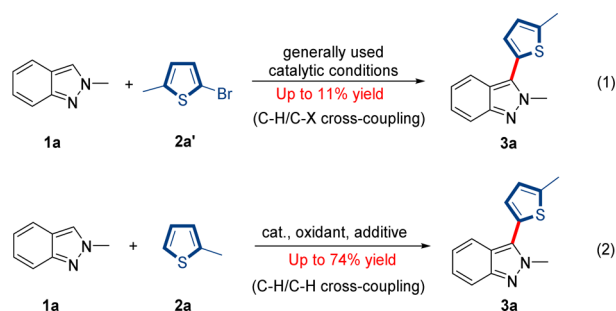
Following our continuous interest in oxidative coupling reactions,[17] we turned our efforts to the oxidative C–H/C–H cross-coupling of 2-methyl-2H-indazole **1a** with various electron-rich heteroarenes. This reaction was investigated by using 2-methylthiophene **2a** as the model substrate (eq 2). At the outset, the biheteroarene **3a** was obtained in 24% yield by employing 5 mol % of Pd(OAc)$_2$ as the catalyst and 1.5 equiv of Cu(OAc)$_2$·H$_2$O as the oxidant in 1,4-dioxane at 120 °C for 24 h (Table S2, entry 1). After screening of several additives, pyridine improved the yield to 70% (Table S2, entries 2−7). After investigating other parameters such as solvents, Pd sources and oxidants (Table S2, entries 10−18), we finally obtained 74% yield under the catalytic system comprising Pd(PPh$_3$)$_4$ (5 mol %), Cu(OAc)$_2$·H$_2$O (1.5 equiv), and

(1)

(2)

Scheme 2. Direct Oxidative C–H/C–H Cross-Coupling of 2H-Indazoles with Various Electron-Rich Heteroarenes and Photophysical Data of the Resulting Catalytic Products[a,b]

3a: 74%
398 nm[e], 0.06[f]
396 nm[g], 0.05[h]

3b: 64%
394 nm[e], 0.39[f]
396 nm[g], 0.35[h]

3c: 33%[c]
414 nm[e], 0.48[f]
420 nm[g], 0.39[h]

3d: 70%
426 nm[e], 0.34[f]
428 nm[g], 0.27[h]

3e: 83%
434 nm[e], 0.30[f]
441 nm[g], 0.22[h]

3f: 33%[c]
434 nm[e], 0.25[f]
438 nm[g], 0.12[h]

3g: 90%
431 nm[e], 0.22[f]
437 nm[g], 0.11[h]

3h: 81%
401 nm[e], 0.55[f]
399 nm[g], 0.56[h]

3i: 67%
398 nm[e], 0.40[f]
396 nm[g], 0.31[h]

3j: 64%
393 nm[e], 0.68[f]
390 nm[g], 0.65[h]

3k: 80%
420 nm[e], 0.10[f]
417 nm[g], 0.05[h]

4a: 68%
410 nm[e], 0.05[f]
409 nm[g], 0.05[h]

4b: 63%
411 nm[e], 0.31[f]
409 nm[g], 0.30[h]

4c: 34%[c]
426 nm[e], 0.48[f]
429 nm[g], 0.30[h]

4d: 76%
453 nm[e], 0.75[f]
458 nm[g], 0.68[h]

4e: 75%
469 nm[e], 0.83[f]
473 nm[g], 0.73[h]

4f: 65%
426 nm[e], 0.47[f]
429 nm[g], 0.53[h]

4g: 78%
499 nm[e], 0.30[f]
509 nm[g], 0.32[h]

5a: 62%
459 nm[e], 0.17[f]
465 nm[g], 0.17[h]

5b: 44%[d]
454 nm[e], 0.74[f]
457 nm[g], 0.35[h]

5c: 30%[c]
455 nm[e], 0.57[f]
458 nm[g], 0.48[h]

5d: 65%[d]
555 nm[e], 0.58[f]
576 nm[g], 0.14[h]

5e: 59%
584 nm[e], 0.14[f]
602 nm[g], ~ 0.01[h]

5f: 60%[d]
508 nm[e], 0.93[f]
525 nm[g], 0.67[h]

5g: 55%
624 nm[e], ~ 0.01[f]
n. d.[g], n. d.[h]

6a: 81%
447 nm[e], 0.26[f]
451 nm[g], 0.24[h]

6b: 71%
449 nm[e], 0.60[f]
457nm[g], 0.51[h]

6c: 59%[c]
472 nm[e], 0.90[f]
490 nm[g], 0.82[h]

6d: 82%
414 nm[e], 0.29[f]
416 nm[g], 0.24[h]

6e: 70%
423 nm[e], 0.16[f]
426 nm[g], 0.15[h]

6f: 67%
456 nm[e], 0.14[f]
454 nm[g], 0.10[h]

6g: 35%
468 nm[e], 0.65[f]
479 nm[g], 0.47[h]

7a: 70%
523 nm[e], 0.37[f]
539 nm[g], 0.18[h]

7b: 93%
525 nm[e], 0.30[f]
542 nm[g], 0.17[h]

7c: 98%
554 nm[e], 0.14[f]
566 nm[g], 0.06[h]

7d: 92%
590 nm[e], 0.03[f]
605 nm[g], ~ 0.01[h]

7e: 88%
602 nm[e], ~ 0.01[f]
632 nm[g], ~ 0.01[h]

8a: 78%
456 nm[e], 0.90[f]
463 nm[g], 0.80[h]

8b: 72%
446 nm[e], 0.86[f]
456 nm[g], 0.81[h]

8c: 84%
443 nm[e], 0.70[f]
444 nm[g], 0.66[h]

[a]Reaction conditions: 2H-indazole (0.25 mmol), electron-rich heteroarene (0.75 mmol), Pd(PPh$_3$)$_4$ (5 mol %), Cu(OAc)$_2$·H$_2$O (1.5 equiv), pyridine (1.0 equiv) and 1,4-dioxane (0.5 mL) at 120 °C for 24 h under N$_2$ atmosphere. [b]Isolated yield. [c]Ten mole percent of Pd(PPh$_3$)$_4$ was used for 36 h. [d]36 h. [e]Emission maximum in CH$_2$Cl$_2$ at 10.0 μM. [f]Absolute quantum yield in CH$_2$Cl$_2$ at 10.0 μM determined with an integrating sphere system. [g]Emission maximum in CH$_3$CN at 10.0 μM. [h]Absolute quantum yield in CH$_3$CN at 10.0 μM determined with an integrating sphere system; n.d., not detected.

pyridine (1.0 equiv) in 1,4-dioxane at 120 °C for 24 h (Table S2, entry 16).

Under the optimized conditions, the scopes of indazoles and electron-rich heteroarenes were tested as summarized in Scheme 2. To our delight, various indazoles could directly couple with a variety of electron-rich heteroarenes such as thiophene, benzothiophene, furan, benzofuran, pyrrole, and indole in moderate to excellent yields. It was also delightful to observe that the protocol well tolerated the functional groups such as aldehyde, acyl, ester, amide, nitro, dimethylamino, methoxy, chloro, and even hydroxyl under the reaction conditions, which could be conveniently modified for the purpose of fluorescence–structure relationship study. Thus, our methodology opens a door for the diversity-oriented construction of C3-heteroarylated 2H-indazole Het[ER]–Het[ED] skeletons.

Fluorescence–structure Relationship. With a divergent library of 3-heteroarylated 2H-indazoles in hand, their photophysical properties including absorptions, excitations, emissions, and quantum yields were measured (for details, see Section III in Supporting Information). It is worth noting that these D–A type fluorophores, named Indazo-Fluors, present full-color-tunable emissions (λ_{em}: 393−624 nm in CH_2Cl_2; 390−632 nm in CH_3CN) with large Stokes shifts (up to 8705 cm^{-1} in CH_2Cl_2; 9177 cm^{-1} in CH_3CN) and high fluorescence quantum yields (up to 93% in CH_2Cl_2; 82% in CH_3CN) (Scheme 2, Figure 4, and Tables S3 and S4).


Figure 4. Photographic images of selected Indazo-Fluors in CH_2Cl_2 (excited at 365 nm under a UV lamp).

To clarify the fluorescence-structure relationship of Indazo-Fluors, the representative data are listed in Tables 1 and 2. First, the quantum yields of Indazo-Fluors are significantly dependent on the electron-rich heteroaryl parts. The Indazo-Fluors composed of thienyl and furanyl moieties have similar emission wavelengths, but the latter possess much higher quantum yields (Table 1). When benzothienyl and benzofuranyl are employed, the analogues of thienyl and furanyl moieties with a larger conjugation, the corresponding Indazo-Fluors gain much higher quantum yields with only tiny variation of emission wavelengths. For instance, **3a** exhibits an emission maximum at 398 nm with a quantum yield of 6%, while its furanyl/benzothienyl counterparts **3b**/**3i** show the similar emission maxima with approximately 7-fold-increased quantum yields (up to 40%).

As reported by Ellman et al.,[14c] the R[1] group at the N2 position has little influence on both absorption and emission wavelengths. **3e** (R[1] = methyl), **3f** (R[1] = phenyl), and **3g** (R[1] = pyridinyl) exhibit similar absorptions (367, 370, and 368 nm, respectively) and emission wavelengths (434, 434, and 431 nm, respectively) in CH_2Cl_2. In addition, their quantum yields are also comparable.

Table 1. Effect of Electron-Rich Heteroaryl Parts on the Photophysical Property of Indazo-Fluors[a]
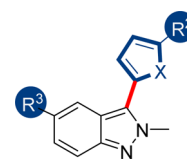
compd	R[2]	R[3]	X	λ_{abs} (nm)	λ_{em} (nm)	Stokes shift (cm^{-1})	Φ_F
3a	Me	H	S	327	398	5455	0.06
3b	Me	H	O	338	394	4205	0.39
3i	benzo	H	S	332	398	4995	0.40
3j	benzo	H	O	345	393	3540	0.68
4a	Me	OMe	S	334	410	5550	0.05
4b	Me	OMe	O	343	411	4824	0.31
4g	CHO	OMe	S	388	499	5733	0.30
4e	CHO	OMe	O	377	469	5203	0.83
5a	Me	N(Me)$_2$	S	364	459	5686	0.17
5b	ME	N(Me)$_2$	O	368	454	5147	0.74
6a	Me	COMe	S	351	447	6119	0.26
6b	Me	COMe	O	365	449	5126	0.60
6g	OMe	COMe	S	358	468	6565	0.65
6c	OMe	COMe	O	375	472	5480	0.90

[a]Photophysical properties in CH_2Cl_2 at 10.0 μM.

Table 2. Effect of Substitutents (R[2] and R[3]) on the Photophysical Property of Indazo-Fluors[a]
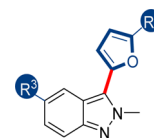

compd	R[2]	R[3]	λ_{abs} (nm)	λ_{em} (nm)	Stokes shift (cm^{-1})	Φ_F
3b	Me	H	338	394	4205	0.39
4b	Me	OMe	343	411	4824	0.31
5b	Me	N(Me)$_2$	368	454	5147	0.74
3c	OMe	H	344	414	4915	0.48
4c	OMe	OMe	348	426	5261	0.48
5c	OMe	N(Me)$_2$	370	455	5049	0.57
6d	COMe	COMe	371	414	2800	0.29
3d	COMe	H	359	426	4381	0.34
4d	COMe	OMe	368	453	5099	0.75
5d	COMe	N(Me)$_2$	407	555	6552	0.58
6e	CHO	COMe	376	423	2955	0.16
3e	CHO	H	367	434	4206	0.30
4e	CHO	OMe	377	469	5203	0.83
5e	CHO	N(Me)$_2$	420	584	6686	0.14

[a]Photophysical properties in CH_2Cl_2 at 10.0 μM.

Subsequently, the impact of the R[2] substituent was investigated. As shown in Table 2, an increase in the electron-withdrawing ability from methyl (**3b**) to acetyl (**3d**) and aldehyde (**3e**)[18] enables bathochromic shifts of emission wavelengths from 394 to 426 and 434 nm, respectively. Thus, it is reasonable to deduce that an even stronger electron-withdrawing R[2] substituent would push the emission even further. As expected, Indazo-Fluor **3l** with an extremely electron-withdrawing dicyanovinyl (DCV) group, which was easily obtained from the Knoevenagel condensation of **3e** with

malononitrile (eq 3),[19] emits yellow fluorescence with a maximum emission of 537 nm in CH_2Cl_2 (Table S3).
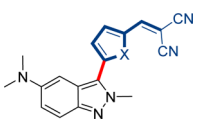

(3)
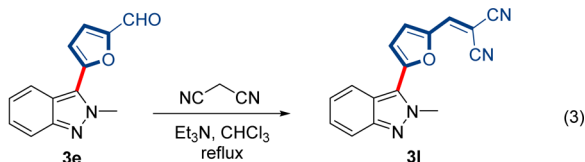
Compared with **3e** (λ_{em} = 434 nm), **3l** shows a large bathochromic shift of 103 nm. It is noteworthy that **3l** exhibits a NIR emission (λ_{em} = 725 nm, Φ_F = 0.05) in the solid state. To the best of our knowledge, **3l** is the lowest molecular weight NIR fluorophore (FW = 274) with emission wavelength over 720 nm in the solid state.[20]

Besides the R^2 substituent, the emissions of Indazo-Fluors are also largely controlled by the electronic nature of the R^3 substituent (Table 2). Taking aldehyde as the reference R^2 substituent, the alteration of the R^3 substituent from electron-withdrawing acetyl (**6e**) to hydrogen (**3e**), methoxy (**4e**), and strong electron-donating N,N-dimethylamino (DMA) (**5e**) induces an obvious bathochromic shift of emission wavelengths from 423 to 434, 469, and 584 nm, respectively. Indazo-Fluors with other R^2 substituents also exhibit such a similar variation tendency of emission wavelengths.

The above study elucidates that (1) the direct connection of intrinsically electron-deficient indazoles and electron-rich heteroarenes quickly establishes a full-color tunable library of Indazo-Fluors; (2) fine tuning of the core skeleton with a strong electron-donating group (D) on the indazole side (R^3) and a strong electron-withdrawing group (A) on the electron-rich heteroaryl side (R^2) could efficiently push the emission of Indazo-Fluors toward red region; and (3) the assembly of a D−Het^{ED}−Het^{ER}−A structure could be considered as an optimal protocol to construct NIR Indazo-Fluors.

Molecular Tuning to NIR Emission. With the optimal pathway to NIR Indazo-Fluors in hand, the aldehyde-bearing fluorophores **5e** and **5g** with the emission maxima at 584 and 624 nm in CH_2Cl_2 were chosen for further modification. The Knoevenagel condensation of **5e** and **5g** with malononitrile afforded **5h** and **5i** with the extremely electron-withdrawing DCV group, which emitted NIR fluorescence at 709 and 710 nm in CH_2Cl_2, respectively (Table 3). It needs to be noted that the molecular weights of **5h** and **5i** are only 317 and 333, respectively. The measurement of photophysical properties reveals that the solvent polarity has little effect on the absorption of **5h**, while the emission of **5h** is significantly red-shifted with attenuated quantum yield with an increase of

the solvent polarity (Figure S1). For example, **5h** exhibits an emission maximum of 609 nm with an absolute quantum yield of 45% in CCl_4, while its emission maximum bathochromically shifts to 709 nm and the quantum yield decreases to approximately 1% in CH_2Cl_2. A similar solvatochromic effect is observed for **5i** as well. These phenomena together with the D−Het^{ED}−Het^{ER}−A structure suggest that **5h** and **5i** might be ICT fluorophores.

The low fluorescence quantum yields of **5h** and **5i** in CH_2Cl_2 could be ascribed to their intrinsic low energy gaps between ground and exited states[21] and the free intramolecular rotation of the biheteroaryl skeletons that dissipates the excited state energy through nonradiative pathway. The free intramolecular rotation could be suppressed effectively when the fluorophore is dispersed in a solid matrix, thus leading to an increased fluorescence. For example, the poly(methyl methacrylate) (PMMA) thin films doped with 0.1 wt % of **5h** or **5i** exhibit absolute quantum yields of 17% and 13%, respectively (Table 3).

To confirm the ICT effect, **5h** was subjected to the density functional theory (DFT) calculation at B3LYP/6-31G(d) level (for details, see Section IV in Supporting Information).[22] The highest occupied molecular orbital (HOMO) is primarily localized over the DMA-substituted indazole moiety, while the lowest unoccupied molecular orbital (LUMO) is mostly centered on the DCV-substituted furanyl moiety (Figure 5).
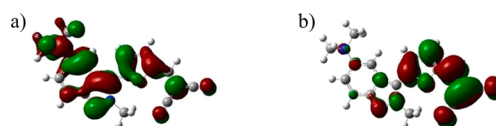

Figure 5. HOMO (a) and LUMO (b) diagrams of **5h**.

Meanwhile, the fluorescent lifetime of **5h**, as measured to be 1.67 ns, is much longer than the solvent orientational relaxation time. Therefore, the evaluation of the dipole moment change ($\Delta\mu = \mu_e - \mu_g$) between the ground state and the excited state could be conducted through solvatochromic effect.[23] A good linear correlation (R = 0.992) is established between the solvent polarity and the Stokes shift (Figure 6), which allows us to
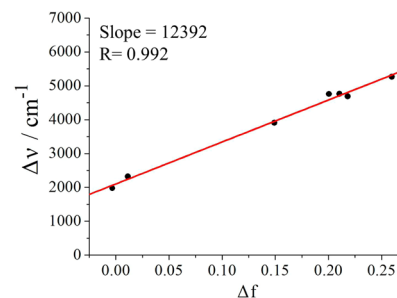

Figure 6. Plot of the Stokes shift ($\Delta\nu$) versus the solvent polarity function (Δf) for **5h**.

calculate the dipole moment change ($\Delta\mu$) of **5h** from the ground state to the excited state. The Onsager radius of 4.982 Å, estimated from quantum chemical calculation by using DFT method at B3LYP/6-31G(d) level,[23f] is used as an effective radius of the solvent cavity for **5h**. The $\Delta\mu$ value was then calculated to be 11.38 D (for details, see Section IV in Supporting Information). Both the DFT calculation and a large

Table 3. Photophysical Properties of 5h and 5i[a]

compd	X	$\lambda_{abs}/\lambda_{ex}$ (nm)	λ_{em} (nm)/Φ_F[b] in CH_2Cl_2	λ_{em} (nm)/Φ_F[b] in PMMA
5h	O	531/533	709/∼0.01	652/0.17
5i	S	535/530	710/∼0.01	644/0.13

[a]Photophysical properties in CH_2Cl_2 (10.0 μM) and PMMA films doped with 0.1 wt % of **5h** or **5i**. [b]Absolute quantum yield determined with an integrating sphere system.

value of $\Delta\mu$ clearly indicate that **5h** is a typical D−A type fluorophore with significant ICT character.

Specific Targeting to Mitochondria. Fluorescent probes have emerged as a powerful tool for noninvasive imaging of various biological processes. With an Indazo-Fluor library in hand, Indazo-Fluors were screened for the confocal fluorescent imaging of HepG2 cell (human hepatocellular liver carcinoma cell line). Living HepG2 cells were cultivated with Indazo-Fluors in PBS (phosphate buffered solution) containing 1% DMSO for 2 h at 37 °C after being cultured in Dulbecco's mimimum eagle's medium (DMEM, containing 10% of fetal bovine serum (FBS), 100 IU mL^{-1} of penicillin, and 100 mg mL^{-1} of streptomycin). To our delight, NIR fluorophore **5h** successfully penetrated the cell membranes and labeled HepG2 cells with a bright red luminescence (Figure 7b). Although both
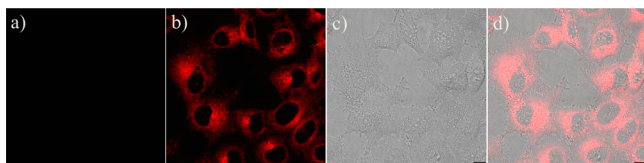
Figure 7. Confocal fluorescence images of HepG2 cells cultured with **5h** in PBS containing 1% DMSO (20.0 μM, λ_{ex} = 552 nm, λ_{em} = 650−750 nm): (a) **5h** without HepG2 cells; (b) **5h** with HepG2 cells; (c) bright-field image; and (d) merged image of (b and c).

of NIR fluorophores **5h** and **5i** were stable in CH$_2$Cl$_2$ under xenon lamp irradiation (Figure S2), the fluorescence of **5i** was rapidly bleached under high-energy laser irradiation. It needs to be noted that the negligible emission of **5h** in PBS (high polar solution) (Figure 7a) could just be thought of as an advantage for a fluorescent bioprobe because it does not bring out any background fluorescence.

Subcellular structures have close ties to normal cellular functions and disease progression.[24] As an important organelle, mitochondria are the energy factory of eukaryotic cells and are also involved in signaling, regulation of metabolism, control of cell cycle, and cellular differentiation as well as cell growth and death.[25] Consequently, it is highly demanding to develop specifically mitochondria-targeted trackers to monitor the mitochondrial functions.[26] Recently, a large number of mitochondria-targeted fluorescent probes have been reported.[27] To further explore the imaging potential of **5h**, subcellular localization experiments with HepG2 cells were performed. Morphological observations showed that **5h** might be localized in mitochondria. Co-staining experiments of HepG2 cells with **5h** and commercially available MitoTracker Green FM (a widely used mitochondria-specific green-fluorescent tracker, **MTG**) were conducted and the images from channel 1 (green luminescence from **MTG**) and channel 2 (red luminescence from **5h**) overlapped very well (Figure 8 and Figure S5). The Pearson's coefficient (R_r = 0.89) and the Manders' coefficients (m_1 = 0.99 and m_2 = 0.90), calculated using Image-Pro Plus software,[28,29] clearly demonstrated the specific accumulation of **5h** into the mitochondria of living cells.[30] Although the exact mechanism of the specific fluorescent imaging of **5h** toward mitochondria is still unclear at current stage, considering its low quantum yield in polar solvent as well as enhanced emission in PMMA film, it is probably ascribed to certain specific interactions between **5h** and mitochondria that restrict intramolecular rotation to result in fluorescence activation of **5h** and further light up mitochondria of HepG2 cells.
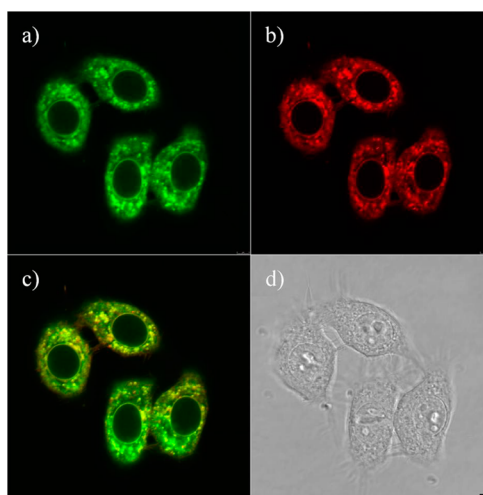

Figure 8. Co-staining of HepG2 cells with **5h** and a commercially available mitochondria-specific tracker **MTG**: (a) fluorescent image of HepG2 cells stained with **MTG** (λ_{ex} = 488 nm, λ_{em} = 500−540 nm); (b) fluorescent image of HepG2 cells stained with **5h** (20.0 μM, λ_{ex} = 552 nm, λ_{em} = 650−750 nm); (c) merged image of (a and b); and (d) bright-field image.

From the application point of view, photostability is a crucial criterion for evaluating a living cell imaging reagent. The high-energy laser beam of confocal microscope may lead to the irreversible destruction of an excited fluorophore (photobleaching). Thus, the photobleaching process often becomes the primary factor limiting the detectability of a fluorescent probe. Typically, commercially available mitochondria trackers suffer from poor photostability.[27d,31] To further evaluate the potential of **5h**, the photostability of **5h** was measured quantitatively together with two well-known commercially available mitochondria-targeted trackers, **MTG** and MitoTracker Red FM (**MTR**). The HepG2 cells stained with them, respectively, were irradiated continuously with unified laser beams under confocal microscope. The initial fluorescence intensities of intracellular **5h**, **MTG**, and **MTR** were normalized and the percentages of the fluorescent signal loss were calculated subsequently (Figure 9). Indazo-Fluor **5h** exhibits almost constant fluorescence intensity and no obvious signal loss during 50 scans with a total irradiation time of about 4 min
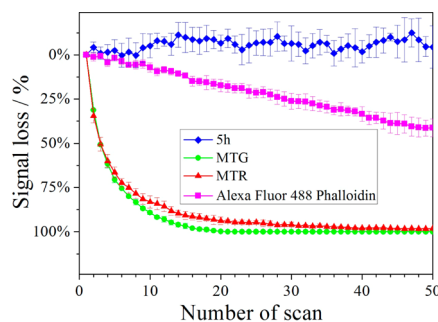

Figure 9. Signal loss (%) of fluorescent emission of **5h** (20.0 μM) in PBS containing 1% DMSO, **MTG**, **MTR**, and Alexa Fluor 488 Phalloidin in living HepG2 cells with increasing number of scans using confocal microscope (irradiation time: 5.14 s/scan). For **5h**, λ_{ex} = 552 nm, λ_{em} = 650−750 nm; for **MTG**, λ_{ex} = 488 nm, λ_{em} = 500−570 nm; for **MTR**, λ_{ex} = 552 nm, λ_{em} = 600−700 nm; for Alexa Fluor 488 Phalloidin, λ_{ex} = 488 nm, λ_{em} = 500−570 nm.
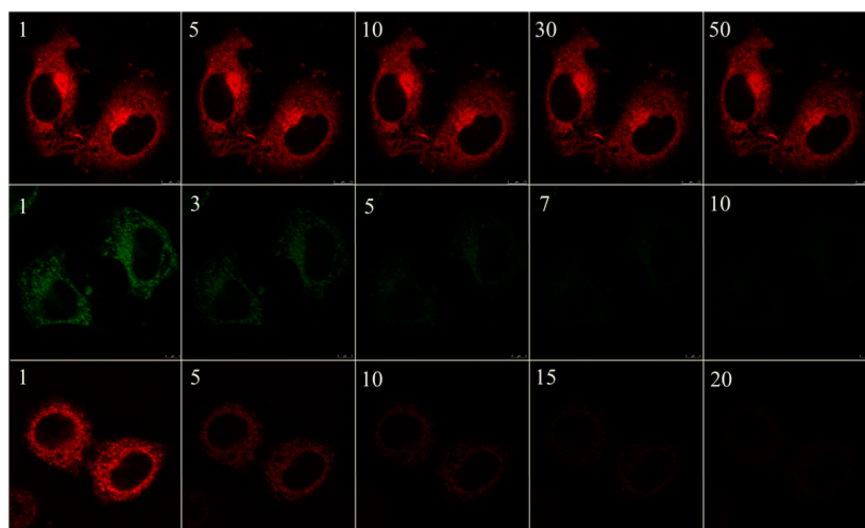
Figure 10. Confocal fluorescence images of HepG2 cells cultured with **5h** (top), **MTG** (middle), and **MTR** (bottom) with increasing number of scans (irradiation time: 5.14 s/scan; the number of scans shown in upper left corner). For excitation wavelengths and emission filters, see Figure 9.

(Figure 10 and Video S1). In contrast, the signal intensities of **MTG** and **MTR** decay steeply during the same time period, and only less than 25% signal intensities remain after the first 10 scans. After 25 scans, the signal intensities of **MTG** and **MTR** almost vanish completely (Figure 10, Video S2 and Video S3). Notably, Alexa Fluor 488 Phalloidin, a representative photostable dye for cytoskeleton imaging, was also used for comparison. The signal intensity of Alexa Fluor 488 Phalloidin decreases to approximately 60% after 50 scans (Figure 9, Figure S6 and Video S4). These results demonstrate that Indazo-Fluor **5h** has superior photostability.[32]

Cytotoxicity is another important factor for a living cell imaging bioprobe. To evaluate the cytotoxicity of **5h**, the comparative experiments among **5h**, **MTG** and **MTR** were conducted in three HepG2 cell lines by using CCK-8 (Cell Counting Kit-8) assays. As shown in Figure 11, **5h** exhibits

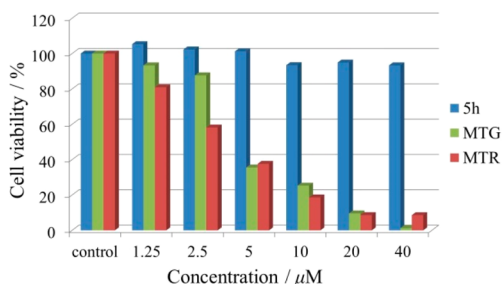biheteroaryl fluorophores (Indazo-Fluors) via a palladium-catalyzed oxidative C−H/C−H cross-coupling reaction of electron-deficient 2H-indazoles with electron-rich heteroarenes. These directly coupled biheteroaryl fluorophores exhibit full-color tunable fluorescence, high quantum yields up to 93%, and large Stokes shifts up to 8705 cm^{-1} in CH_2Cl_2. Further fine-tuning of the core skeleton successfully pushes the emission wavelengths over 700 nm. The protocol developed herein opens a door to rapidly screen minimal NIR-emitting fluorophores.

The obtained Indazo-Fluor **3l** is the smallest NIR fluorophore with the emission wavelength over 720 nm in the solid state. The NIR dye **5h** specifically lights up mitochondria with bright red luminescence in living cells, and exhibits superior photostability as well as very low cytotoxicity, which would be a prominent candidate as a fluorescent bioimaging reagent toward mitochondria. Although a number of mitochondria-targeted fluorescent probes have been commercialized, the NIR trackers for mitochondria targeting still remain scarce. As far as we know, **5h** is the smallest NIR probe with specific targeting to mitochondria. The easy access to Indazo-Fluors developed herein has well exemplified the great appeal of C−H activation and unlocks an opportunity in high-throughput, modulated screening for specific functional molecules.

Figure 11. Cell viability values (%) estimated by CCK-8 assays using HepG2 cells, cultured in the presence of 1.25−40 μM of **5h**, **MTG**, and **MTR** for 24 h at 37 °C, respectively.

almost no toxicity to cultured HepG2 cells. Very little variation of cell viability is observed even with the higher concentration of **5h** at 40 μM. In sharp contrast, the cell viabilities decrease significantly with a gradual increase of the concentrations of **MTG** and **MTR**. When the concentrations of **MTG** and **MTR** reach 5 μM, the cell viabilities are less than 40%.

CONCLUSION

In summary, on the basis of the intrinsic electronic property of heteroarenes, we have established a library of D−A type

ASSOCIATED CONTENT

Ⓢ Supporting Information

The Supporting Information is available free of charge on the ACS Publications website at DOI: 10.1021/jacs.5b09241.

> Experimental procedures, characterization data, photo-physical data, computational calculations, cell imaging experiments, cytotoxicity experiments and copies of NMR spectra (PDF)
> Video S1 (AVI)
> Video S2 (AVI)
> Video S3 (AVI)
> Video S4 (AVI)

AUTHOR INFORMATION

Corresponding Authors
*jsyou@scu.edu.cn
*gg2b@scu.edu.cn

Notes
The authors declare no competing financial interest.

ACKNOWLEDGMENTS

REFERENCES

(1) For books and reviews, see: (a) Guilbault, G. G. *Practical fluorescence*, 2nd ed., revised and expanded; Marcel Dekker: New York, 1999. (b) Zhang, J.; Campbell, R. E.; Ting, A. Y.; Tsien, R. Y. *Nat. Rev. Mol. Cell Biol.* **2002**, *3*, 906. (c) Gonçalves, M. S. T. *Chem. Rev.* **2009**, *109*, 190. (d) Kobayashi, H.; Ogawa, M.; Alford, R.; Choyke, P. L.; Urano, Y. *Chem. Rev.* **2010**, *110*, 2620. (e) Li, X.; Gao, X.; Shi, W.; Ma, H. *Chem. Rev.* **2014**, *114*, 590. (f) Tao, Y.; Yuan, K.; Chen, T.; Xu, P.; Li, H.; Cheng, R.; Zheng, C.; Zhang, L.; Huang, W. *Adv. Mater.* **2014**, *26*, 7931.

(2) (a) Chan, J.; Dodani, S. C.; Chang, C. J. *Nat. Chem.* **2012**, *4*, 973. (b) Vendrell, M.; Zhai, D.; Er, J. C.; Chang, Y.-T. *Chem. Rev.* **2012**, *112*, 4391.

(3) (a) *Near-Infrared Applications in Biotechnology*; Raghavachari, R., Ed.; Marcel Dekker: New York, 2001. (b) Weissleder, R. *Nat. Biotechnol.* **2001**, *19*, 316. (c) Frangioni, J. V. *Curr. Opin. Chem. Biol.* **2003**, *7*, 626. (d) Hilderbrand, S. A.; Weissleder, R. *Curr. Opin. Chem. Biol.* **2010**, *14*, 71. (e) Guo, Z.; Park, S.; Yoon, J.; Shin, I. *Chem. Soc. Rev.* **2014**, *43*, 16. For selected examples, see: (f) Lukinavičius, G.; Umezawa, K.; Olivier, N.; Honigmann, A.; Yang, G.; Plass, T.; Mueller, V.; Reymond, L.; Corrêa, I. R., Jr; Luo, Z.-G.; Schultz, C.; Lemke, E. A.; Heppenstall, P.; Eggeling, C.; Manley, S.; Johnsson, K. *Nat. Chem.* **2013**, *5*, 132. (g) Choi, H. S.; Gibbs, S. L.; Lee, J. H.; Kim, S. H.; Ashitate, Y.; Liu, F.; Hyun, H.; Park, G.; Xie, Y.; Bae, S.; Henary, M.; Frangioni, J. V. *Nat. Biotechnol.* **2013**, *31*, 148.

(4) (a) Chen, W.; Wright, B. D.; Pang, Y. *Chem. Commun.* **2012**, *48*, 3824. (b) Cui, M.; Ono, M.; Watanabe, H.; Kimura, H.; Liu, B.; Saji, H. *J. Am. Chem. Soc.* **2014**, *136*, 3388.

(5) (a) Ando, Y.; Niwa, K.; Yamada, N.; Enomoto, T.; Irie, T.; Kubota, H.; Ohmiya, Y.; Akiyama, H. *Nat. Photonics* **2008**, *2*, 44. (b) Naumov, P.; Ozawa, Y.; Ohkubo, K.; Fukuzumi, S. *J. Am. Chem. Soc.* **2009**, *131*, 11590.

(6) (a) Nesterov, E. E.; Skoch, J.; Hyman, B. T.; Klunk, W. E.; Bacskai, B. J.; Swager, T. M. *Angew. Chem., Int. Ed.* **2005**, *44*, 5452. (b) Wakamiya, A.; Taniguchi, T.; Yamaguchi, S. *Angew. Chem., Int. Ed.* **2006**, *45*, 3170. (c) Park, H. J.; Lim, C. S.; Kim, E. S.; Han, J. H.; Lee, T. H.; Chun, H. J.; Cho, B. R. *Angew. Chem., Int. Ed.* **2012**, *51*, 2673. (d) Fukazawa, A.; Kishi, D.; Tanaka, Y.; Seki, S.; Yamaguchi, S. *Angew. Chem., Int. Ed.* **2013**, *52*, 12091. (e) Kim, G. H.; Halder, D.; Park, J.; Namkung, W.; Shin, I. *Angew. Chem., Int. Ed.* **2014**, *53*, 9271.

(7) Johnson, I.; Spence, M. T. Z. *The Molecular Probes Handbook, A Guide to Fluorescent Probes and Labeling Technologies*, 11th ed; Molecular Probes: Eugene, OR, 2010.

(8) (a) Grabowski, Z. R.; Rotkiewicz, K.; Rettig, W. *Chem. Rev.* **2003**, *103*, 3899. (b) Wakamiya, A.; Mori, K.; Yamaguchi, S. *Angew. Chem., Int. Ed.* **2007**, *46*, 4273.

(9) (a) Zhao, Z.; Wang, Z.; Lu, P.; Chan, C. Y. K.; Liu, D.; Lam, J. W. Y.; Sung, H. H. Y.; Williams, I. D.; Ma, Y.; Tang, B. Z. *Angew. Chem., Int. Ed.* **2009**, *48*, 7608. (b) Kim, E.; Koh, M.; Lim, B. J.; Park, S. B. *J. Am. Chem. Soc.* **2011**, *133*, 6642. (c) Karton-Lifshin, N.; Albertazzi, L.; Bendikov, M.; Baran, P. S.; Shabat, D. *J. Am. Chem. Soc.* **2012**, *134*, 20412. (d) Liu, X.; Xu, Z.; Cole, J. M. *J. Phys. Chem. C* **2013**, *117*,

16584. (e) Choi, E. J.; Kim, E.; Lee, Y.; Jo, A.; Park, S. B. *Angew. Chem., Int. Ed.* **2014**, *53*, 1346.

(10) Fujita, M.; Nakao, Y.; Matsunaga, S.; Seiki, M.; Itoh, Y.; Yamashita, J.; van Soest, R. W. M.; Fusetani, N. *J. Am. Chem. Soc.* **2003**, *125*, 15700.

(11) For reviews and highlights, see: (a) Han, W.; Ofial, A. R. *Synlett* **2011**, 1951. (b) Bugaut, X.; Glorius, F. *Angew. Chem., Int. Ed.* **2011**, *50*, 7479. (c) Cho, S. H.; Kim, J. Y.; Kwak, J.; Chang, S. *Chem. Soc. Rev.* **2011**, *40*, 5068. (d) Zhao, D.; You, J.; Hu, C. *Chem. - Eur. J.* **2011**, *17*, 5466. (e) Yeung, C. S.; Dong, V. M. *Chem. Rev.* **2011**, *111*, 1215. (f) Wu, Y.; Wang, J.; Mao, F.; Kwong, F. Y. *Chem. - Asian J.* **2014**, *9*, 26. (g) Hirano, K.; Miura, M. *Chem. Lett.* **2015**, *44*, 868.

(12) (a) Wencel-Delord, J.; Glorius, F. *Nat. Chem.* **2013**, *5*, 369. (b) Segawa, Y.; Maekawa, T.; Itami, K. *Angew. Chem., Int. Ed.* **2015**, *54*, 66.

(13) Schmidt, A.; Beutler, A.; Snovydovych, B. *Eur. J. Org. Chem.* **2008**, 4073.

(14) (a) Ma, F.; Zhou, N.; Zhu, J.; Zhang, W.; Fan, L.; Zhu, X. *Eur. Polym. J.* **2009**, *45*, 2131. (b) Vernekar, S. K. V.; Hallaq, H. Y.; Clarkson, G.; Thompson, A. J.; Silvestri, L.; Lummis, S. C. R.; Lochner, M. *J. Med. Chem.* **2010**, *53*, 2324. (c) Lian, Y.; Bergman, R. G.; Lavis, L. D.; Ellman, J. A. *J. Am. Chem. Soc.* **2013**, *135*, 7122.

(15) Higashiguchi, K.; Matsuda, K.; Asano, Y.; Murakami, A.; Nakamura, S.; Irie, M. *Eur. J. Org. Chem.* **2005**, 91.

(16) For a recent example on direct C3−H heteroaryltion of 2H-indazoles with electron-deficient haloheteroarenes, see: Ohnmacht, S. A.; Culshaw, A. J.; Greaney, M. F. *Org. Lett.* **2010**, *12*, 224.

(17) (a) Xi, P.; Yang, F.; Qin, S.; Zhao, D.; Lan, J.; Gao, G.; Hu, C.; You, J. *J. Am. Chem. Soc.* **2010**, *132*, 1822. (b) Wang, Z.; Li, K.; Zhao, D.; Lan, J.; You, J. *Angew. Chem., Int. Ed.* **2011**, *50*, 5365. (c) Dong, J.; Long, Z.; Song, F.; Wu, N.; Guo, Q.; Lan, J.; You, J. *Angew. Chem., Int. Ed.* **2013**, *52*, 580. (d) Qin, X.; Liu, H.; Qin, D.; Wu, Q.; You, J.; Zhao, D.; Guo, Q.; Huang, X.; Lan, J. *Chem. Sci.* **2013**, *4*, 1964. (e) Liu, B.; Huang, Y.; Lan, J.; Song, F.; You, J. *Chem. Sci.* **2013**, *4*, 2163. (f) Huang, Y.; Wu, D.; Huang, J.; Guo, Q.; Li, J.; You, J. *Angew. Chem., Int. Ed.* **2014**, *53*, 12158. (g) Qin, X.; Li, X.; Huang, Q.; Liu, H.; Wu, D.; Guo, Q.; Lan, J.; Wang, R.; You, J. *Angew. Chem., Int. Ed.* **2015**, *54*, 7167.

(18) (a) Jaffé, H. H. *Chem. Rev.* **1953**, *53*, 191. (b) Szklarska-Smialowska, Z.; Kaminski, M. *Corros. Sci.* **1973**, *13*, 1.

(19) Roquet, S.; Cravino, A.; Leriche, P.; Alévêque, O.; Frère, P.; Roncali, J. *J. Am. Chem. Soc.* **2006**, *128*, 3459.

(20) Investigation of the solid-state fluorescecence of Indazo-Fluors will be reported elsewhere in due course.

(21) (a) Rurack, K.; Spieles, M. *Anal. Chem.* **2011**, *83*, 1232. (b) Zhang, Q.; Kuwabara, H.; Potscavage, W. J., Jr.; Huang, S.; Hatae, Y.; Shibata, T.; Adachi, C. *J. Am. Chem. Soc.* **2014**, *136*, 18070.

(22) (a) Shimizu, M.; Takeda, Y.; Higashi, M.; Hiyama, T. *Angew. Chem., Int. Ed.* **2009**, *48*, 3653. (b) Kubota, Y.; Hara, H.; Tanaka, S.; Funabiki, K.; Matsui, M. *Org. Lett.* **2011**, *13*, 6544. (c) Li, D.; Zhang, H.; Wang, C.; Huang, S.; Guo, J.; Wang, Y. *J. Mater. Chem.* **2012**, *22*, 4319. (d) Shimizu, M.; Kaki, R.; Takeda, Y.; Hiyama, T.; Nagai, N.; Yamagishi, H.; Furutani, H. *Angew. Chem., Int. Ed.* **2012**, *51*, 4095. (e) Yuan, W. Z.; Gong, Y.; Chen, S.; Shen, X. Y.; Lam, J. W. Y.; Lu, P.; Lu, Y.; Wang, Z.; Hu, R.; Xie, N.; Kwok, H. S.; Zhang, Y.; Sun, J. Z.; Tang, B. Z. *Chem. Mater.* **2012**, *24*, 1518.

(23) (a) Lippert, E. Z. *Naturforsch.* **1955**, *10a*, 541. (b) Mataga, N.; Kaifu, Y.; Koizumi, M. *Bull. Chem. Soc. Jpn.* **1955**, *28*, 690. (c) Beens, H.; Knibbe, H.; Weller, A. *J. Chem. Phys.* **1967**, *47*, 1183. (d) Herbich, J.; Kapturkiewicz, A. *J. Am. Chem. Soc.* **1998**, *120*, 1014. (e) Karpiuk, J. *J. Phys. Chem. A* **2004**, *108*, 11183. (f) Gong, Y.; Guo, X.; Wang, S.; Su, H.; Xia, A.; He, Q.; Bai, F. *J. Phys. Chem. A* **2007**, *111*, 5806. (g) Jia, M.; Ma, X.; Yan, L.; Wang, H.; Guo, Q.; Wang, X.; Wang, Y.; Zhan, X.; Xia, A. *J. Phys. Chem. A* **2010**, *114*, 7345.

(24) Satori, C. P.; Henderson, M. M.; Krautkramer, E. A.; Kostal, V.; Distefano, M. M.; Arriaga, E. A. *Chem. Rev.* **2013**, *113*, 2733.

(25) (a) Green, D. R.; Galluzzi, L.; Kroemer, G. *Science* **2011**, *333*, 1109. (b) Nunnari, J.; Suomalainen, A. *Cell* **2012**, *148*, 1145.

(26) (a) Hoye, A. T.; Davoren, J. E.; Wipf, P.; Fink, M. P.; Kagan, V. E. *Acc. Chem. Res.* **2008**, *41*, 87. (b) Yousif, L. F.; Stewart, K. M.; Kelley, S. O. *ChemBioChem* **2009**, *10*, 1939.

(27) For selected examples, see: (a) Kawazoe, Y.; Shimogawa, H.; Sato, A.; Uesugi, M. *Angew. Chem., Int. Ed.* **2011**, *50*, 5478. (b) Zhang, T.; Zhu, X.; Cheng, C. C. W.; Kwok, W.-M.; Tam, H.-L.; Hao, J.; Kwong, D. W. J.; Wong, W.-K.; Wong, K.-L. *J. Am. Chem. Soc.* **2011**, *133*, 20120. (c) Pierroz, V.; Joshi, T.; Leonidova, A.; Mari, C.; Schur, J.; Ott, I.; Spiccia, L.; Ferrari, S.; Gasser, G. *J. Am. Chem. Soc.* **2012**, *134*, 20376. (d) Leung, C. W. T.; Hong, Y.; Chen, S.; Zhao, E.; Lam, J. W. Y.; Tang, B. Z. *J. Am. Chem. Soc.* **2013**, *135*, 62.

(28) Manders, E. M. M.; Verbeek, F. J.; Aten, J. A. *J. Microsc.* **1993**, *169*, 375.

(29) Yu, F.; Li, P.; Wang, B.; Han, K. *J. Am. Chem. Soc.* **2013**, *135*, 7674.

(30) Zinchuk, V.; Zinchuk, O. In *Current Protocols in Cell Biology*; John Wiley & Sons, Inc.: Hoboken, NJ, 2014; Supplement 62, p 4.19.1.

(31) (a) Huang, S.; Han, R.; Zhuang, Q.; Du, L.; Jia, H.; Liu, Y.; Liu, Y. *Biosens. Bioelectron.* **2015**, *71*, 313. (b) Jin, C.; Liu, J.; Chen, Y.; Zeng, L.; Guan, R.; Ouyang, C.; Ji, L.; Chao, H. *Chem. - Eur. J.* **2015**, *21*, 12000.

(32) It is noteworthy that most of Indazo-Fluors show capability to mark HepG2 cells, suggesting the great potential of the Indazo-Fluor library for bioimaging applications. Most Indazo-Fluors show good photostability in HepG2 cells under laser beam of confocal microscope. For selected examples, see Figure S7.